RECENT RESULTS FROM THE OPAL EXPERIMENT*

N.K. WATSON**

CERN, European Organisation for Particle Physics
1211 Geneva 23, Switzerland

(Received October 26, 1992)

After two full years of physics running the OPAL collaboration has observed and analysed approximately 5×10^5 hadronic decays of the Z^0. Many new analyses have been completed since the end of the 1991 physics run, of which three are described in detail. A preliminary study of the electric charge of quark and gluon jets in Z^0 decays is presented. A comprehensive investigation into the value of the strong coupling parameter $\alpha_s(M_{Z^0})$, using 15 different observables from hadronic Z^0 and τ decays, is shown. Event shapes, jet rates and energy correlation are consistently described by the single value $\alpha_s(M_{Z^0}) = 0.122^{+0.006}_{-0.005}$ in $\mathcal{O}(\alpha_s^2)$. The first measurement of two-particle momentum correlations in hadronic Z^0 decays and a comparison of this observable with recent analytic QCD calculations and with Monte Carlo simulations is also described.

PACS numbers: 12.38. Qk

1. Introduction

Since the start of operation of the LEP collider in 1989, there have been two full years of physics data taking at centre of mass energies in the vicinity of the Z^0 resonance. During this time approximately 5×10^5 hadronic decays of the Z^0 have been recorded using the OPAL detector. These data have been used to perform many studies of the standard model of strong and electroweak interactions. The electroweak sector of the model, which is based on the gauge group $SU(2)_L \times U(1)_Y$, has been tested by making precise measurements of the various model parameters and comparing them with hard, theoretical predictions [1].

---

* Presented at the XXXII Cracow School of Theoretical Physics, Zakopane, Poland, June 2–12, 1992.

** Representing the OPAL Collaboration.

In contrast, the strong sector of the standard model, based on the gauge group SU(3), has self-coupling gauge quanta which makes theoretical calculations (and therefore experimental tests of the model) considerably more difficult to perform. Analytic QCD calculations are currently carried out using perturbative methods and are only applicable in the high energy region where the coupling is sufficiently weak for this approach to be valid, which is unfortunately above the energy scale at which observed hadrons are formed. In order to compare experimental data with QCD calculations it is therefore necessary to either restrict the comparison to quantities which are only sensitive to the initial response of the system in the perturbative region, such as the total cross section, or for the behaviour of the non-perturbative region to be modelled in an empirical way. This is the basic problem with trying to test the strong sector of the standard model: there are relatively few predictions because of the complexity of the theory and even those that exist tend to be less precise than the experimental data.

In this report, emphasis is placed on studies into the nature of the strong sector of the standard model. In Section 2, the OPAL dataset used for analyses is summarised and a very brief overview is given of recently completed or ongoing investigations. This is followed by detailed descriptions of three analyses. The first of these, in Section 3, outlines a preliminary study into the electric charge of quark and gluon jets in hadronic Z^0 decays [2]. Section 4 describes a recently published analysis in which many different observables are used to determine $\alpha_s(M_{Z^0})$, and the way in which these measurements constitute an important consistency check of the reliability of perturbative QCD [3]. The last study, presented in Section 5, is a new measurement of two-particle momentum correlations and a comparison with recent analytic QCD calculations and various Monte Carlo models [4]. Finally, closing remarks and comments are made in Section 6.

2. Overview

Before describing analyses in detail, it is instructive for a few remarks to be made about the data on which investigations are based and also to give a flavour for the variety of studies which have been performed recently.

2.1. OPAL Dataset 1989–1992

The most valuable part of an experimental analysis are the data. This is particularly true of an experiment such as OPAL where much effort has gone into ensuring that the best possible use is made of luminosity delivered by the LEP machine. The efficiency for recording Z^0 events in OPAL has increased with each year of running to the current (high) value of approximately 90%, a number which includes the readout deadtime of the detector

itself (typically 2–3%). The data available for analyses at the current time[1] are summarised in Table I.

TABLE I

Evolution of OPAL dataset

	1989	1990	1991	1992
$\int \mathcal{L}\, dt$ recorded, pb^{-1}	1.4	6.8	14.3	≥ 0.9
Hadronic Z^0 decays recorded	30k	150k	350k	≥ 28k
OPAL data taking efficiency	$\approx 70\%$	76%	87%	$\approx 90\%$

Having two full years of running completed, the OPAL experiment [5] may be considered to be mature. After much study, the data recorded during 1990 are well understood which is reflected by small experimental systematic errors. Furthermore, the large dataset allows many studies which have previously been limited by available statistics to be performed.

2.2. Summary of recent analyses

Since the end of the 1991 run, many analyses have been finalised and published [6–10, 3, 11–14, 4]. The quality of these analyses is indicated by presenting a few details from each of three studies. (There are in addition ongoing studies of the Z^0 lineshape, searches for the Higgs boson and so forth but these are not described in this report.)

The first of these is a measurement of $B^0 - \bar{B}^0$ mixing in which the sign of the lepton charge, in events having two charged leptons, is used to tag the charge of the b quark in b-flavoured hadrons [6]. A flavour discriminating variable, p_{comb} is constructed,

$$p_{\mathrm{comb}} = \sqrt{\left(\frac{p}{10}\right)^2 + p_{\mathrm{T}}^2}\,,$$

where p is the lepton momentum, and p_{T} its component perpendicular to the jet axis. The quantity, R, defined as the fraction of selected two lepton events in which both leptons have the same charge, is used to indicate the sensitivity of this measurement to the value of the average mixing parameter, χ.

In Fig. 1, the variation of R as a function of p_{comb} is shown together with predictions for three different values of χ. By fitting the fraction of

[1] Data recorded before 2nd June 1992.

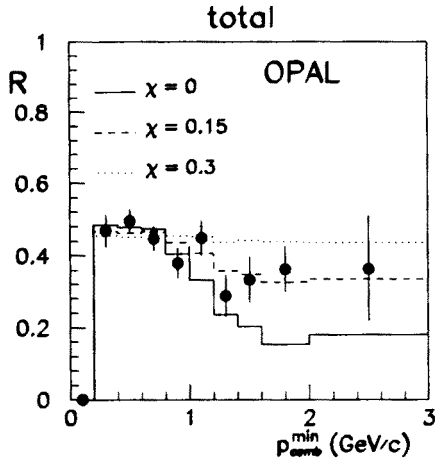

Fig. 1. The fraction, R, of dilepton events which are like sign as a function of p_{comb}, for $\mu\mu$, $e\mu$ and ee events.

events in which the two lepton charges are of the same sign, as a function of this variable, the average mixing parameter is measured to be

$$\chi = 0.145^{+0.041}_{-0.035} \pm 0.018,$$

where the first error is statistical and the second is systematic.

A second interesting analysis is one in which evidence for the production of b-flavoured baryons in Z^0 decays is reported [11]. The evidence relies on the expectation that semi-leptonic decays of b baryons may produce $\Lambda\ell^-$ and $\overline{\Lambda}\ell^+$ ("right sign") combinations but not $\Lambda\ell^+$ and $\overline{\Lambda}\ell^-$ ("wrong sign") ones. This correlation between the sign of the baryon number of a Λ particle with the electric charge[2] of an associated lepton is the signature used to identify b baryon production. The leptons (electrons or muons) are characterised by relatively large momentum and transverse momentum with respect to the primary b hadron direction, whilst the Λ particles are identified by their tendency to have distinctly higher momentum than the background from other fragmentation processes.

The $p\pi^-$ invariant mass distribution of Λ particles for the various combinations of 'Λ' and 'ℓ' are shown in Fig. 2. By restricting the definition of a Λ candidate to $p\pi^-$ combinations that fall within 20 MeV of the nominal Λ mass, a total of 68 "right" sign pairs of Λ particle and associated charged lepton are found in the entire 1990 and 1991 data sample; the excess of signal candidates (Fig. 2(a)) over background events (Fig. 2(b)) is apparent.

[2] Charge conjugation is implied in describing the remainder of this analysis.

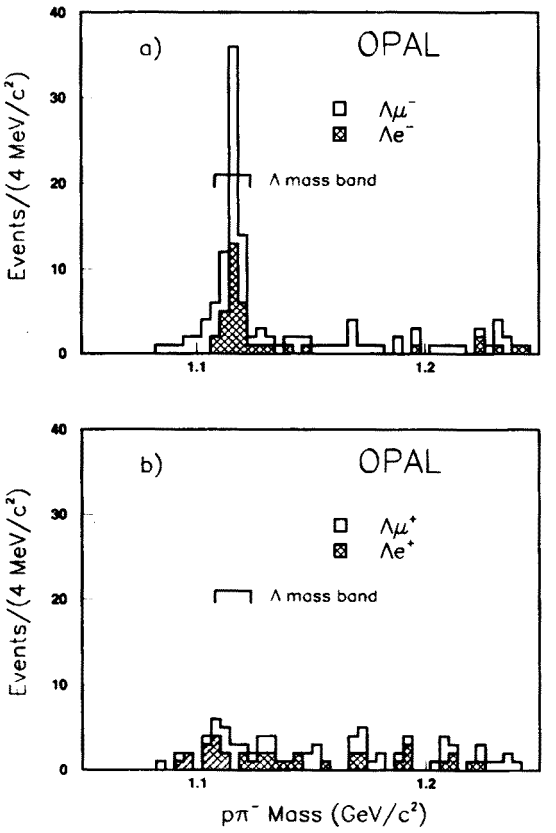

Fig. 2. Invariant mass distributions for Λ particles in "right sign" combinations (a) and "wrong sign" combinations (b).

This is interpreted as a signal of $55 \pm 9^{+0.3}_{-3.1}$ events from the semi-leptonic decay of b baryons.

The last selected analysis is a measurement of the production rate of electrons in hadronic decays of the Z^0 and a determination of $\Gamma(Z^0 \to b\bar{b})$ [12]. The primary decay of b-flavoured hadrons, $b \to e\nu_e X$, is forced to be the dominant source of electrons in a selected sample by the requirements that electrons have momentum, $p > 4$ GeV, and momentum transverse to the axis of the jet containing a given electron, $p_t > 0.8$ GeV. Estimates of the electron identification efficiency and the hadronic background are extracted from the dataset; that these are well understood is illustrated by Fig. 3, which shows the separation of electron candidates from hadronic background as a function of E_{cone}/p, the electromagnetic cluster energy scaled by the charged track momentum.

In order to determine $\Gamma_{b\bar{b}}$, it is assumed that the semi-leptonic branch-

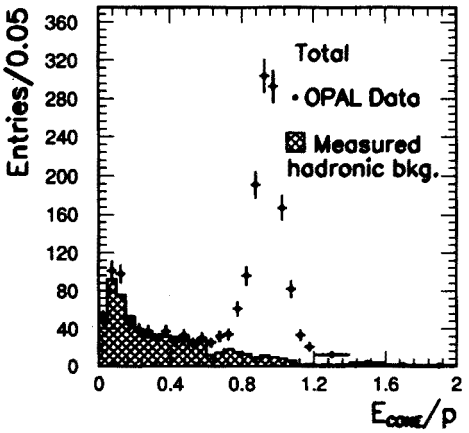

Fig. 3. Estimation of hadronic background; number of events with high momentum electron candidates as a function of $E_{\rm cone}/p$.

ing fraction of hadrons on the Z^0 resonance is the same as the branching fraction measured at the $\Upsilon(4S)$. Correlations between the model dependence of the branching fractions measured at the $\Upsilon(4S)$ and the kinematic acceptance of electrons within OPAL are accounted for, reducing the model dependence of this measurement. The final partial width determined in this study is,

$$\Gamma_{b\bar{b}} = 394 \pm 13 \pm 32\text{MeV}$$

where the largest component of the systematic error is from the uncertainty in the electron identification efficiency.

These extracts from recent studies are representative of the other analyses which have recently been completed. The remainder of this report is devoted to describing three other analyses in more detail.

3. Study of electric charge of quark and gluon jets

This is a *preliminary* study, based on approximately 140 000 hadronic events from the 1990 data sample [2].

3.1. Introduction

Quantum Chromodynamics predicts differences between quark and gluon jets due to the fact that they do not have the same colour charge as one another. An example of such a prediction is the ratio of the charged multiplicity in 3-jet events (final state $q\bar{q}g$) to that in 2-jet events (final state $q\bar{q}$; from naive colour counting considerations this ratio is expected to

be $^{17}/_{8}$.) Further differences are also expected as a result of the different electric charges of quarks and gluons [15]. Experimental studies of the electric charge of jets (the so-called "jet charge") in $p\bar{p}$-collisions have shown that the mean charge of jets originating from the fragmentation of u quarks, $\bar{u}$ quarks and gluons were positive, negative and zero respectively. In this study, the first preliminary investigation of jet charge in e^+e^- collisions at the centre of mass energies, $\sqrt{s} \simeq 91$ GeV is made.

Being able to distinguish quark jets from gluon jets and also being able to identify the sign of the primary quark charge in a given jet are central to this analysis. This is achieved by selecting 3-jet events containing an energetic, charged lepton and making cuts based on event kinematics and assuming the charged lepton originates from the semi-leptonic decay of a heavy quark. The sign of the charged lepton is used to form enriched samples of jets originating from positively and negatively charged primary quarks. The jet charges are then constructed on an event by event basis for each of 239 events which satisfy the above selection criteria. Various hypotheses are tested against the data. It is found that the mean jet charge of the quark jets is incompatible with zero, the sign of the jet charge is as expected from the sign of the primary quark, and the mean charge of the gluon jet is compatible with zero.

The following Sections describe the experimental event selection criteria and the way in which enriched samples of quark and gluon jets are formed, consideration of backgrounds, the construction of the jet charge and analysis of the distributions extracted from the data, and studies of systematic effects. Finally, a summary of the results is made and conclusions are drawn.

3.2. Event selection

This analysis depends upon being able to distinguish between quark and gluon jets and uses essentially the same method as employed in previous publications [16, 17]. Cuts are applied to select planar, 3-jet events that are fully contained within the acceptance of the detector. This process may be considered in three stages. In the first of these, events are required to satisfy:

- The number of charged tracks > 9.
- The sum of charged track and neutral cluster energy, $E_{\mathrm{vis}} > 0.5\sqrt{s}$.
- The angle between beam axis, $\vec{z}$, and thrust axis, $\vec{T}$, $> 30°$.
- All charged track 3-momenta, $|\vec{p}_i| < 60$ GeV.
- In both hemishperes (defined by plane $\perp \vec{T}$), the invariant mass > 2 GeV.
- One charged lepton with 3-momentum, $|\vec{p}| > 3$ GeV (μ) or $|\vec{p}| > 2$ GeV (e).

In the second stage, events are retained if they consist of three jets, where the jet classification is defined according to the JADE algorithm in the p recombination scheme [18], with a resolution scale, $y_{\mathrm{cut}} = 0.03$. For completeness, the p scheme defines the resolution parameter, y, and recombination of pseudo-particles:

$$\text{resolution:} \quad y = \frac{(p_i + p_j)^2}{s},$$

$$\text{recombination:} \quad \begin{cases} \vec{p}_{ij} = \vec{p}_i + \vec{p}_j \\ E_{ij} = |\vec{p}_{ij}| \end{cases},$$

where E is the energy and subscripts i, j and ij refer to pseudo-particles i, j and the new pseudo-particle formed by combining i and j, respectively.

The third stage rejects events which do not satisfy the criteria:

- For each *jet*, the sum of charged track and neutral cluster energy, $E_{\mathrm{vis}}^{\mathrm{jet}} > 5$ GeV.
- The event must be planar, *i.e.* the sum of the three inter-jet angles $> 358°$.
- The angle between the beam axis and each jet axis, $> 25°$.
- The number of charged particles in each jet > 4.
- The jet with the highest $\sum_i |\vec{p}_i|$, *i.e.* the energy of a jet as defined in the p scheme, must not contain the charged lepton. (i runs over all particles in a jet.)

Having selected a sample of well measured, 3-jet events each jet is identified as originating from either a primary quark or a gluon as below.

3.3. Identification of quark and gluon jets

In a 3-jet event, it is argued that the most energetic jet is unlikely to be the gluon jet as the gluon has been radiated from one of the primary quarks. The most energetic jet (the "highest energy jet") is therefore assigned to arise from one of the primary quarks. The energetic, charged lepton is assumed to originate from the semi-leptonic decay of a heavy quark. Assuming that gluon fragmentation into heavy quarks is a negligible contribution as a consequence of the high mass, the jet which contains the charged lepton (the "lepton jet") is taken as originating from the second primary quark. The third jet by a process of elimination is defined to be the gluon jet. In order to increase the purity of these associations, the additional requirement that the highest energy jet must have at least 8 GeV more energy than the gluon jet is imposed.

These associations are supported by Monte Carlo studies carried out using the JETSET [19] program[3] and a full simulation of the OPAL detec-

[3] Model parameters from [20] are used.

tor [21]. The probabilities that the highest energy jet, the lepton jet and the gluon jet assignments are correct is estimated to be 90%, 92% and 83%, respectively. From the initial sample of 140 189 events, 735 remain at this stage in the analysis.

In order to make tests based on the jet charge, it is necessary to know the sign of the primary quark charge in one of the jets in each event. By assuming that the charged lepton is the result of the semi-leptonic decay of a heavy quark, *i.e.* $b^{-1/3} \rightarrow c^{+2/3}\ell^{-}\nu_{\ell}$, it follows that the sign of the primary quark is the same as that of the charged lepton. Consequently, the events are divided into two samples according to the sign of the lepton charge. However, there are various background processes which may lead to the lepton charge having a sign different to the primary quark in a given event which have to be addressed.

3.4. Background reduction

The main processes whereby the sign of the lepton charge is different from that of the primary quark are cascade decays, $B^0 - \bar{B}^0$ mixing, π or K decays which may emulate muons, and Dalitz decays or photo-conversions which may be mis-identified as primary electrons. The contribution from these sources may be reduced by making use of the relatively hard momentum spectrum of the charged leptons from the decay of heavy quarks, and rejecting events in which the momentum of the lepton with respect to the jet axis, $p_{\perp}^{\text{lepton}} < 1$ GeV. The lepton is included in the calculation of the jet axis.

Monte Carlo studies (including detector simulation) lead to the estimate that 70% of leptons selected are from prompt b quark decays and that there is an 87% probability that the lepton will have the same sign charge as the primary quark. In 'background' events, the sign of the lepton candidate is often the same as that of the primary quark, as such relatively high momentum particles reflect the properties of the primary quark. The simulation indicates that the $p_{\perp}^{\text{lepton}}$ cut, whilst removing most cascade decays, has no significant effect on the estimated purities for the jet assignments. The effect of $B^0 - \bar{B}^0$ mixing, which is not simulated by the Monte Carlo, is estimated to lead to the wrong sign charge being deduced for the primary quark in the order of 5% of events [6].

The $p_{\perp}^{\text{lepton}}$ cut removes around 70% of the sample, leaving 239 events for the jet charge study. It should be noted that the purities and efficiencies estimated from Monte Carlo are given for information only and the subsequent analysis does not depend upon their precise values.

3.5. Jet charge definition

The jet charge, Q, used in this analysis is constructed:

$$Q = \frac{1}{\langle p_{\parallel}^{\kappa} \rangle} \sum_{i}^{N} q_i \, p_{\parallel i}^{\kappa} \quad \text{with} \quad \langle p_{\parallel}^{\kappa} \rangle = \frac{1}{N} \sum_{i}^{N} p_{\parallel i}^{\kappa},$$

where N is the number of charged particles in a given jet, and q_i, $p_{\parallel i}^{\kappa}$ are respectively the charge and the momentum component along the jet axis of particle i. This form for jet charge has been used by earlier experiments [22, 23] and found to have sensitivity to the sign of the charge of the parton from which the jet in question was formed. The normalisation present in this definition of Q reduces the sensitivity to the jet energy. The jet charge for a given jet is not constrained to have integral multiples of the electron charge.

The probability, P_Q, that Q and the underlying parton in a jet have the same sign as each other is a quantitative indicator of the sensitivity of jet charge as an observable. The optimal choice of the parameter, κ, which is present in the definition of Q is studied using Monte Carlo. The range considered is $0.1 < \kappa < 2.0$. For large κ, Q is most influenced by high momentum particles — for the lepton jet, P_Q increases with κ, as the lepton which carries information about the charge of the primary quark has increased weight. No such effect is seen for the highest energy jet. Although the precise value of P_Q is not important, it is preferable to have approximately the same value of P_Q for both highest energy jets and lepton jets. The compromise between sensitivity to the lepton charge and minimising differences between lepton and highest energy jets is $\kappa = 0.2$. With this κ, $|Q|$ is typically less than five units of charge.

For information only, P_Q is estimated from the data, by considering the number of events in which both quark jets have the same jet charge and the number of events in which both quark jets have the opposite charge. The probability, P_Q is estimated to be approximately 70%, which is sufficiently high that meaningful comparisons between jet charge and the charge of the partons can be made.

3.6. Analysis of jet charge distributions

The selected sample of 239 events, which is divided into two categories according to the sign of lepton charge, is analysed as follows. The subsample of events in which the lepton has a negative charge are considered first. It was proposed earlier that the lepton was formed during the semi-leptonic decay of a heavy quark and so one expects the sign of the lepton

to be the same as that of the primary quark in the same jet. Given that the jet charge has been shown empirically to be sensitive to the sign of the underlying parton charge in a jet, it is expected that the frequency distribution for jet charge from negatively charged lepton jets will be shifted to negative values. This is clearly seen in the part of Fig. 4(a) that refers to negative lepton tags ("ℓ^--jet").

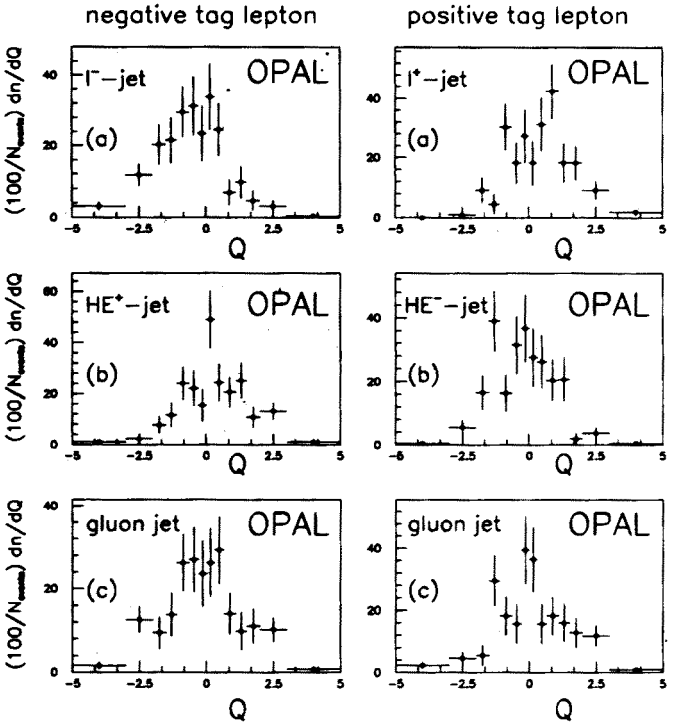

Fig. 4. Jet charge distributions for events with a negative lepton (left) and a positive lepton (right), for (a) lepton jets, (b) highest energy jets, (c) gluon jets.

Still concentrating on this sub-sample of events, the highest energy jet is proposed to be the other quark jet in each event, and so it is expected to have the opposite charge sign to the (negative) lepton jet. This is shown in Fig. 4(b), as "HE$^+$-jet", and is also shifted in the sense expected. The Q for the third jet in each event of this sub-sample, the gluon jet, is displayed in Fig. 4(c), and is compatible with being centred at zero.

The same distributions are also formed for the positively charged lepton sub-sample, as shown in Fig. 4, in the column labelled "positive tag lepton". These are expected to be shifted to the opposite sign of Q with respect to the negatively charged lepton sub-sample described above, which is what is seen from the figure. As these two sets of distributions are consistent with each other, the positively charged lepton sub-sample is reflected through

$Q = 0$ and combined with the corresponding distributions in the other subsample. It is stressed that no corrections from Monte Carlo studies have been applied to the data at any point in the analysis.

TABLE II

Jet charge distributions of combined data

	$\langle Q \rangle$
lepton jet	-0.68 ± 0.12
highest energy jet	$+0.41 \pm 0.12$
gluon jet	-0.11 ± 0.13

The mean values of the jet charge in each of these combined distributions is given in Table II. Given these measured values, the following hypotheses are proposed and tested:

- The jet charge of the lepton jet and the gluon jet have a common mean: this hypothesis has a χ^2/d.o.f. of 9.8/1.
- The jet charge of the highest energy jet and the gluon jet have a common mean: this hypothesis has a χ^2/d.o.f. of 8.1/1.
- The jet charge of all jets have a common mean: this hypothesis has a χ^2/d.o.f. of 39.0/2.

3.6.1. Systematic effects

Numerous systematic checks have been carried out during this study, as detailed below. The form for the jet charge itself is a potential source of systematic bias, as it lends itself to being unduly influenced by the presence of high momentum and transverse momentum particles in a jet. In a Monte Carlo study, the jet charge distributions were examined for gluon and highest energy jets in samples with and without energetic hadrons that satisfy the kinematic cuts applied to the leptons. No systematic variation is observed.

The analysis was repeated using events which contained two lepton tagged jets, which gives a higher purity to the detriment of efficiency. Although the size of the sample is smaller, the result is entirely compatible with the single lepton tag sample.

The energy dependence of the jet charge is also considered. The average jet energies (in the data) for the highest energy jet, the lepton jet and the gluon jet are found to be 35.3 GeV, 26.1 GeV and 13.8 GeV, respectively. For each type of jet, the mean value of $\langle Q \rangle$ is evaluated separately for events above and below the mean value of Q. No dependence is observed in any case. In a Monte Carlo study, it is found that $|\langle Q \rangle|$ decreases slowly with

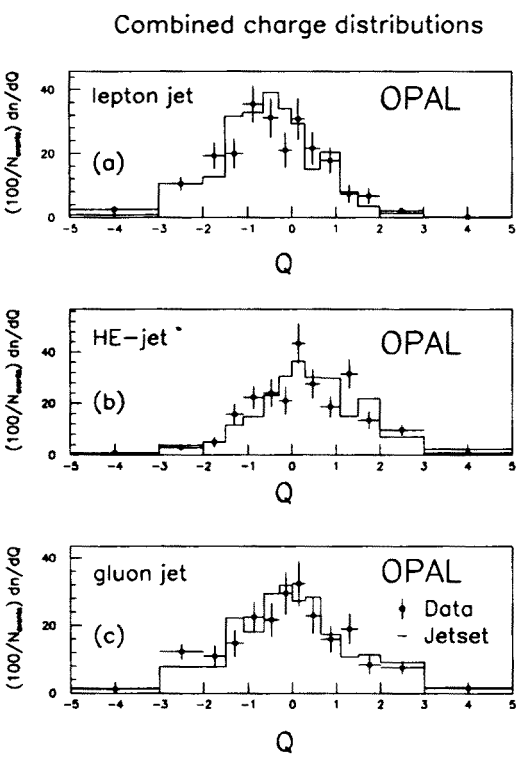

Fig. 5. Combined jet charge distributions for events, as in Fig. 4. Points represent OPAL data, solid histogram is Monte Carlo.

decreasing jet energy for the quark jets, but as there is no such effect for the gluon jets this is unlikely to explain any differences observed,

For illustration only, the combined jet charge distributions are given in Fig. 5. Good agreement is seen between the Monte Carlo simulation (solid histogram) and the measured data. A final consistency check performed is to repeat the analysis for the Monte Carlo data with detector simulation, but to obtain the identity of the underlying parton in all jets from the 4-vectors generated, thus allowing the jet charge to be determined using perfect quark and gluon separation and perfect quark charge identification. The mean jet charges so obtained are shifted by approximately 1.5 standard deviations farther away from $Q = 0$ than for the case where parton assignments are made in the same way as for the real data. This is entirely as expected as this procedure removes all events in which the wrong jet charge assignment is made.

3.7. *Summary and conclusions*

This analysis has selected a sample of 239 planar, 3-jet events with a single high momentum and transverse momentum charged lepton per event, at $\sqrt{s} \simeq 91$ GeV. Quark and gluon jets have been separated and samples of jets enriched with positively and negatively charged quarks have been selected using lepton tagging and energy ordering. It has been observed that: the mean jet charge of quark jets is incompatible with zero by more than three standard deviations; the sign of the jet charge for quark jets corresponds to expectation from the sign of the charged lepton tag; the mean jet charge of the gluon jet is entirely compatible with zero; and the hypothesis that the highest energy jet of the lepton jet has a mean jet charge which is compatible with the gluon jet has a χ^2/d.o.f. greater than 8.1/1.

It is concluded that the significant difference in the jet charge distributions of quarks gluons is caused by the different electric charges of quarks and gluons.

4. Measurement of strong coupling parameter, $\alpha_s(M_{Z^0})$

This is a published analysis, based on approximately 140 000 hadronic events from the 1990 data sample. Full details are available in the literature [3].

4.1. *Introduction*

The fundamental coupling parameter of QCD, α_s is much less well measured than its counterparts in the electroweak sector of the standard model. In this study, α_s is determined from a study of 15 different physical observables. As the determination of α_s for each observable is in general subject to different sources of systematic uncertainty (mainly theoretical), these measurements complement each other. A feature of QCD is that there is only one coupling parameter in the theory which must describe all data if the theory is correct. The converse of this, that α_s determinations made using any observable must yield the same value of α_s, allows the result of this study to be interpreted as a significant test of the consistency of perturbative QCD.

It is found that when theoretical uncertainties (including the choice of the renormalisation scale) are taken into account, all measurements may be described by a single value of $\alpha_s(M_{Z^0}) = 0.122^{+0.006}_{-0.005}$ in $\mathcal{O}(\alpha_s^2)$.

The remainder of this Section lists all of the observables studied and the order of the theoretical predictions which are available for each. This is followed by an outline of the general method used to extract α_s from

data for the specific case of an $\mathcal{O}(\alpha_s^2)$ theoretical prediction; the treatment of systematic errors is summarised and the determination of α_s from jet rates is given to illustrate a typical $\mathcal{O}(\alpha_s^2)$ measurement. Having described a single measurement, the method whereby the 12 different $\mathcal{O}(\alpha_s^2)$ determinations are combined is presented. Subsequent Sections deal in turn with the determination of α_s using resummed next-to-leading order logarithmic calculations and also $\mathcal{O}(\alpha_s^3)$ calculations, where an example is given in both cases. Finally, the many measurements are summarised and conclusions are drawn.

4.1.1. Observables

The observables used in this study include event shape variables, jet masses, jet rates, energy correlations, Z^0 line shape parameters and τ lepton branching ratios; various theoretical calculations exists for the different observables. The quantities studied, each of which is defined in [3], may be categorised according to the type of calculations used, as given below.

- Calculations to $\mathcal{O}(\alpha_s^2)$ [24, 25] are used for:
  Event shape variables
  C-parameter, C,
  Oblateness, O,
  Thrust, T,
  Jet masses
  Heavier jet mass (to thrust axis), M_H^T
  Difference jet mass (to thrust axis), M_D^T
  Heavier jet mass (to minimised axis), M_H^M
  Difference jet mass (to minimised axis), M_D^M
  Jet rates (JADE algorithm)
  E0 recombination scheme,
  D (Durham) recombination scheme,
  p recombination scheme,
  E recombination scheme,
  Energy correlations
  Asymmetry of energy-energy correlation, AEEC
  Planar triple energy correlation, PTEC
- Calculations which include resummation of leading and next-to-leading logarithms to all orders in α_s [26, 27], matched to the $\mathcal{O}(\alpha_s^2)$ calculations are used for:
  Event shape variables
  Thrust, T,
  Jet masses
  Heavier jet mass (to thrust axis), M_H^T
  Heavier jet mass (to minimised axis), M_H^M

- Calculations to $\mathcal{O}(\alpha_s^3)$ [28–30] are used for:
  Z^0 line shape
  Z^0 partial width and line shape
  τ lepton branching ratios

4.2. Determinations of α_s based on $\mathcal{O}(\alpha_s^2)$ QCD

Theoretical predictions which are valid to $\mathcal{O}(\alpha_s^2)$ are available for many observables [24, 25]. It is on these calculations that the majority of the α_s determinations presented here are based. There are many features of these different analyses which are common to all and it is these aspects which are now addressed.

Consider the determination of α_s using a generic observable, X. The differential cross section for this quantity, to $\mathcal{O}(\alpha_s^2)$, may be written

$$\frac{1}{\sigma_{\rm tot}}\frac{d\sigma}{dX} = \frac{\alpha_s(\mu)}{2\pi}A(X) + \left(\frac{\alpha_s(\mu)}{2\pi}\right)^2 \left(A(X)2\pi b_0 \ln(x_\mu^2) + B(X)\right), \quad (1)$$

with

$$b_0 = \frac{1}{12\pi}(33 - 2n_f); \quad \sigma_{\rm tot} = \sigma_0\left[1 + \frac{\alpha_s}{\pi} + 1.41\left(\frac{\alpha_s}{\pi}\right)^2\right],$$

where n_f is the number of active quark flavours (assumed to be five), and $\sigma_{\rm tot}$ and σ_0 represent the total hadronic and the leading order cross sections for $e^+e^- \to$ hadrons, respectively. The functional forms of $A(X)$ and $B(X)$ have been determined [24] by evaluating the $\mathcal{O}(\alpha_s^2)$ matrix elements of [25]. The parameter μ characterises the renormalisation scale dependence.

It is important to notice that whilst *infinite* order calculations are independent of the scale parameter, μ, finite order calculations (beyond $\mathcal{O}(\alpha_s)$) have explicit dependence on the choice of μ. Whilst there exist various theoretical prescriptions for the choosing the value of μ (*e.g.* [31–34], there is no general agreement on the preferred procedure and each scheme may predict a different μ for each observable. As the value of α_s determined depends on the scale chosen, the effect of varying μ is taken into account in the final determination. This "scale uncertainty" (*i.e.* is choice of μ) is regarded as a source of theoretical systematic error.

4.2.1. Comparison of data and QCD predictions

The expression for the observable X given in Eq. (1) describes a distribution for massless partons, whereas the experimental distribution is constructed using massive hadrons, with many additional effects from detector

resolution and acceptance, initial state radiation, *etc.* It is therefore necessary to "correct" the experimental distributions to allow for these effects before a meaningful comparison can be made. This is done in two steps using a simple bin-by-bin procedure.

The first correction is for detector effects and initial state radiation. Distributions of X are constructed using two samples of Monte Carlo data, one consisting of final state hadrons without simulation of initial state radiation (the *hadron level*), the other consisting of final state hadrons including the effects of measurement with the OPAL detector and initial state radiation (the *detector level*). ("Detector level" means that a very detailed simulation of OPAL [21] has been used; exactly the same event reconstruction and analysis algorithms are applied to the simulated events as to real data.) Comparing these two simulated distributions leads to a set of correction factors which allow the data to be unfolded for both detector and ISR effects to the hadron level.

The second correction which is applied is to account for the effects of hadronisation. In this case, a procedure analogous to the previous correction is used. The difference here is that the Monte Carlo samples compared are for final state hadrons without initial state radiation and for partons before hadronisation occurs. By making these corrections the distribution of X at the parton level is extracted from the experimental data. The final stage of the comparison is to fit[4] the expression in Eq. (1) to the corrected data, and obtain a value for α_s.

4.2.2. Treatment of systematic errors

Owing to the large size of the OPAL dataset, statistical errors rarely dominate the overall uncertainty on α_s. The difficulty is in evaluating the various systematic errors and understanding the way in which they might bias the central value of α_s. Here, an attempt is made to outline the sources of systematic error considered and the magnitude of the effect attributed to each.

The first systematic error considered is that which results from detector related effects. It is estimated to contribute a systematic uncertainty $\Delta\alpha_s \sim \mathcal{O}(0.001)$ to a given α_s determination. The validity of the unfolding procedure depends upon the detector simulation providing an accurate description of the experiment; this is seen to be the case [20]. The effects of small, residual deficiencies which may exist in the simulation are estimated by performing each analysis (where applicable) using each of charged tracks alone, electromagnetic clusters alone and finally both charged tracks and

[4] In practise, such fits are normally performed for $\Lambda_{\overline{MS}}$, the result of which is used to determine α_s, using the expression from [37], given in Eq. (2).

electromagnetic clusters. The central value for α_s is that obtained using the latter method and the largest difference between any of the three techniques is assigned to be the systematic error from detector effects.

The second systematic error considered arises from the uncertainties in the hadronisation process and the correction procedure used to account for it. A systematic uncertainty in the range $\Delta\alpha_s \sim \mathcal{O}(0.001) - \mathcal{O}(0.01)$ is typically attributed to a given measurement from this source. The hadronisation corrections are actually derived by comparing hadron level and parton level distributions using three different Monte Carlo models, *viz.* JETSET 7.2 [19], HERWIG 5.0 [35] and COJETS 6.12 [36]. The central value is that derived from the JETSET corrections (JETSET gives the best description of data at the detector level) and the differences between the models are used to estimate the error. Where only JETSET describes the data, uncertainties are estimated by varying model parameters in the Monte Carlo. Further effects arise from the choice of the virtuality scale of the partons, which defines the boundary between the perturbative and hadronisation phases in the parton shower models, and from evaluating hadronisation corrections using a $\mathcal{O}(\alpha_s^2)$ matrix element calculation [25] within JETSET.

The next source of systematic error considered is the choice of the range of X within which a fit to the theoretical prediction is made. The uncertainty from this source is estimated to contribute a systematic uncertainty $\Delta\alpha_s \sim \mathcal{O}(0.001)$ to a given α_s determination. A standard range is defined for each observable, inside which the detector correction is acceptably uniform and the hadronisation correction is not too large. Fits are performed separately within this range; where significant differences are found with respect to the results from the standard fit range, the systematic error is inflated so as to account for discrepancies.

The last and largest systematic error considered is that attributed to the uncertainty in the choice of the renormalisation scale, μ. This uncertainty, which is theoretical in origin, typically contributes $\Delta\alpha_s \sim \mathcal{O}(0.01)$ to the systematic error on a measurement of α_s. A useful quantity to introduce is the renormalisation scale factor, x_μ, defined,

$$\mu = x_\mu \sqrt{s}\,.$$

For the observable, X, values for $\alpha_s(M_{Z^0})$ are determined with $x_\mu = 1$ and with x_μ a free parameter in the fit. Allowing x_μ to vary freely should indicate the "natural" scale for the observable in question. The average of these two determinations gives the central value of $\alpha_s(M_{Z^0})$, whilst half of their difference gives the systematic uncertainty from the choice of scale. An alternative to this method, which is used where the fitted value of $x_\mu \simeq 1$, is to base the scale error upon the range of x_μ values for which an acceptable χ^2/d.o.f. for the fit is possible; this is to avoid an unrealistically small scale uncertainty being attributed to a measurement.

It is worth noting that all α_s results given are for $\alpha_s(\mu = M_{Z0})$, *i.e.* the $\Lambda_{\overline{MS}}$ from each fit is substituted in the expression (*e.g.* from [37]),

$$\alpha_s(\mu) = \frac{12\pi}{(33-2n_f)\ln\left(\frac{\mu^2}{\Lambda^2_{\overline{MS}}}\right)}\left[1 - \frac{6(153-19n_f)}{(33-2n_f)^2}\frac{\ln\left[\ln\left(\frac{\mu^2}{\Lambda^2_{\overline{MS}}}\right)\right]}{\ln\left(\frac{\mu^2}{\Lambda^2_{\overline{MS}}}\right)}\right], \quad (2)$$

with $\mu = M_{Z0}$.

Having described the general procedures common to many analyses, it is interesting to see how they are applied in practise, as below.

4.2.3. Example of $\mathcal{O}(\alpha_s^2)$ determination of α_s: jet rates

Jet production rates have often been used in the past to determine the strong coupling parameter (see [18] and references therein). A jet finding scheme is used in order to compare theoretical prediction with data, as it is a well-defined method which is calculable in perturbation theory and also experimentally tractable. In $\mathcal{O}(\alpha_s^2)$, the relative rate of 3-jets to the total cross section provides a direct measurement of α_s. It is functionally similar to Eq. (1), with the jet resolution parameter, y, which is usually some variant of the invariant mass of a pair of particles or jets, replacing the generic observable, X. The jet rate is based on a successive recombination scheme (JADE type algorithm, [38]) whereby particles i, j are combined to form jets ij in an iterative manner until all jet masses satisfy a criteria of the form, $y_{ij} > y_{\rm cut}$, where $y_{\rm cut}$ is some arbitrary, fixed value.

The success of this type of algorithm stems from the fact that jet rates so defined are relatively insensitive to hadronisation effects. The drawback with this procedure is that there may be sizable perturbative corrections from uncalculated higher order terms in the expansions. This is indicated by the non-negligible scale dependence associated with these measurements. Another problem associated with such jet schemes is that at small values of y, fits to the data tend to favour improbably small values of the renormalisation scale, μ. This is indicative of the emergence of large logarithms in y at each order in perturbation theory [39], and is a fundamental theoretical problem.

Two possible solutions to these problems are to either calculate the jet rates to higher order in perturbation theory, which is is non-trivial, or to find a new jet definition which has reduced higher order effects and better theoretical behaviour. A recently proposed jet finding scheme, the Durham or D scheme, [40], appears to satisfy this latter criteria. Experimental results obtained using this new jet finding algorithm are presented here for the first time.

In the D scheme, the jet resolution parameter is defined by,

$$y_{ij} = \frac{2.\min(E_i^2, E_j^2)(1 - \cos\theta_{ij})}{s},$$

where E_i, E_j and θ_{ij} represent the energy of jets i and j, and the angle between jets i and j. This parameter is based upon the relative transverse momentum of jets, rather than on the minimum invariant mass of jets as with previous definitions of this type. Furthermore, it allows the resummation to all orders in α_s of leading and next-to-leading logarithms of y for the small y region. Only the fixed order predictions will be discussed here for this observable; although the resummed calculations appear promising they are not used for this observable[5] here.

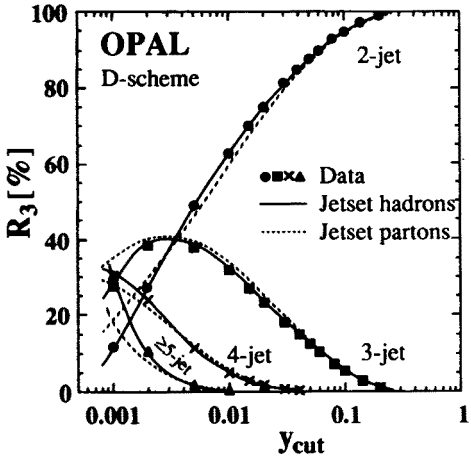

Fig. 6. Relative production rates of n-jet events using the Durham jet finding algorithm. The data are corrected for detector effects but not for hadronisation.

The relative production rates of n-jet events measured using the D scheme, $R_n(y)$, are given in Fig. 6, where the data have been corrected for detector effects such as resolution and acceptance only. No hadronisation effects have been unfolded from the data. Also presented in the figure are the n-jet rates for the JETSET parton shower Monte Carlo with string fragmentation. It is clear that the model describes the data well and also that the difference predicted between hadron level and parton level results by the Monte Carlo are relatively small, as hoped for in the D scheme.

[5] At the time this analysis was submitted for publication, these calculations were not finalised.

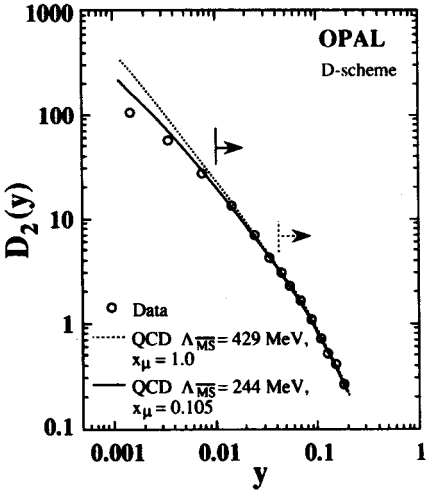

Fig. 7. Differential 2-jet rates defined in the Durham scheme. The data are corrected for detector and hadronisation effects. The QCD predictions are shown along with the corresponding fit ranges.

However, as all events appear at each value of $y_{\rm cut}$, adjacent bins of this distribution are not independent which is not ideal if one wishes to fit a prediction to this distribution.

The differential 2-jet distribution, $D_2(y)$, which measures the y value at which each event changes from being classed as 3-jet to 2-jet, is used to extract α_s from the jet production rates and is shown in Fig. 7. It is defined,

$$D_2(y) = \frac{R_2(y) - R_2(y - \Delta y)}{\Delta y},$$

where $R_2(y)$ is the relative 2-jet fraction at y and Δy is the interval in y considered. Each event appears only once in the distribution which makes fitting the theoretical prediction to the data more convenient. The data given in the figure have been corrected for both detector and hadronisation effects. Theoretical curves are given for two fits, one for a fit in which the renormalisation parameter was fixed at $x_\mu = 1$, the other for a fit in which it was allowed to vary freely. The corresponding standard fit ranges are also shown.

The final coupling determined from this particular investigation is found to be,

$$\alpha_s(M_{Z^0}) = 0.125^{+0.008}_{-0.007} \qquad \text{Durham scheme},$$

where the uncertainty given includes statistical and systematic errors added

TABLE III

Systematic uncertainties contributing to error on $\alpha_s(M_{Z^0})$ from differential 2-jet rates in Durham scheme.

Source of uncertainty	Error
statistical	± 0.001
experimental (detector effects)	± 0.004
hadronisation	± 0.001
virtuality cut-off in model	$^{+0.004}_{-0.000}$
renormalisation scale	± 0.006
Total uncertainty	$^{+0.008}_{-0.007}$

in quadrature. The individual systematic errors contributing to this uncertainty are presented in Table III. As expected, the renormalisation scale dependence is the dominant error.

4.3. Combination of $\mathcal{O}(\alpha_s^2)$ measurements

The differential 2-jet rate in the Durham scheme is one typical observable used to determine α_s in $\mathcal{O}(\alpha_s^2)$. A more reliable estimate of α_s is made by combining the measurements made using the different observables, as some cancellations are expected between the various uncertainties. However, the complicated correlations which exist between the individual measurements mean that there is no unique way of combining the measurements; two different techniques were studied.

The first method is to perform combined fits, in which various sets of observables (e.g jet rates, event shapes) are fitted with a common value of $\Lambda_{\overline{MS}}$ and either: a common value of $x_\mu = 1$; or a common, freely varying x_μ; or a freely varying x_μ for each observable. The fits with a common x_μ can not accommodate all of the data, in contrast to those in which each observable is fitted with a separate x_μ. In the latter case, the higher order corrections are accounted for by allowing each observable to adjust to the preferred scale. The large variation in x_μ which result from this procedure is illustrated in the lower half of Fig. 8; the preferred scale for most observables tends to be the point at which α_s is minimal, as can be seen in the upper half of this figure.

The second method is to construct the weighted average of the individual measurements, $\bar{\alpha}_s$. In order to estimate the systematic uncertainty on this central value, the total errors for each source of uncertainty are added in quadrature. The "total" errors are constructed using weighted averages, *e.g.* for the hadronisation error, one value, $\bar{\alpha}_s$, is evaluated using JETSET,

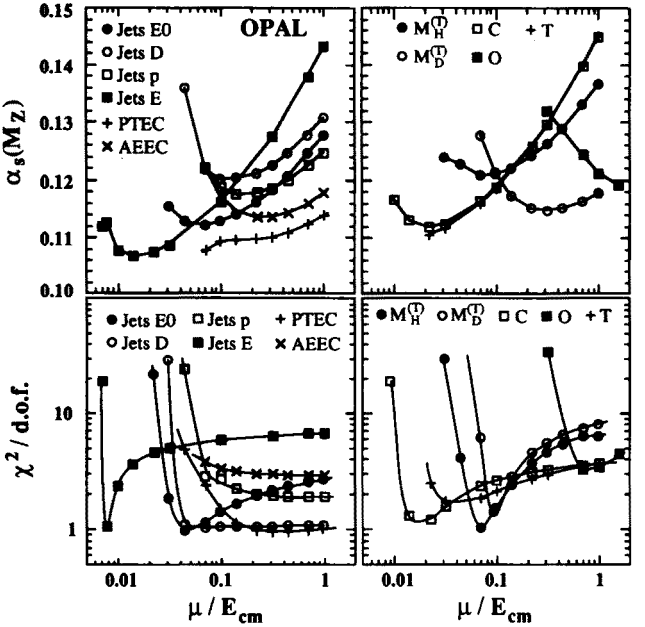

Fig. 8. Dependence of α_s and χ^2/d.o.f. of fits on the renormalisation scale factor, x_μ.

another value, $\bar{\alpha}_s'$, is determined using HERWIG and the difference $\bar{\alpha}_s - \bar{\alpha}_s'$ gives the corresponding total error.

The values determined for α_s in $\mathcal{O}(\alpha_s^2)$ by these two techniques are,

$$\begin{aligned} &\text{Combined fit,} && \alpha_s(M_{Z^0}) = 0.118^{+0.007}_{-0.008}\,, \\ &\text{Weighted average,} && \alpha_s(M_{Z^0}) = 0.122^{+0.005}_{-0.006} \end{aligned}$$

which are entirely consistent, the combined fit being slightly lower as each individual α_s is evaluated at the preferred x_μ, which tends to be at the minimum value of α_s.

4.4. Determination of α_s based on resummed QCD calculations

The limiting factor in the above determinations is the lack of calculations beyond $\mathcal{O}(\alpha_s^2)$, which is apparent in the scale dependence of the results. It was recently shown possible [26, 27] (for certain observables) to resum all terms in the perturbative expansion having the form,

$$\alpha_s^n \ln^m \left(\frac{M_H}{s}\right), \qquad \text{for } m \geq n\,.$$

This is the basis of the so-called next-to-leading logarithm approximation, NLLA. These calculations are expected to give an improvement over fixed order ones at lower jet masses. The calculations are matched to the exact $\mathcal{O}(\alpha_s^2)$ matrix elements, resulting in calculations with full matrix elements for all terms up to $\mathcal{O}(\alpha_s^2)$ and also leading and next-to-leading logarithmic terms for all orders beyond $\mathcal{O}(\alpha_s^2)$. Such calculations are used for the observables $M_H^{(T)}$, $M_H^{(M)}$ and T, giving an overall result of,

$$\mathcal{O}(\alpha_s^2)\text{+resummed NLLA}, \qquad \alpha_s(M_{Z^0}) = 0.122^{+0.003}_{-0.006}$$

4.4.1. Example of resummed determination of α_s: heavier jet mass

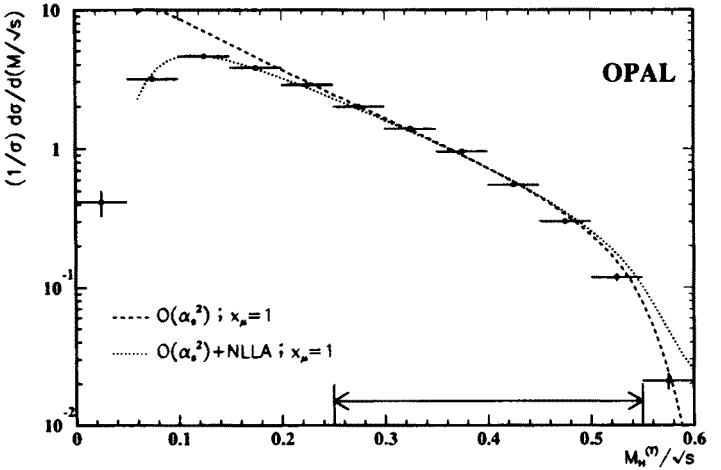

Fig. 9. Distribution of $M_H^{(T)}$ compared with fits to the $\mathcal{O}(\alpha_s^2)$ and to the matched $\mathcal{O}(\alpha_s^2)$ + NLLA calculations, with scale $x_\mu = 1$. The arrow indicates the fit range.

In order to demonstrate the improvement obtained with this procedure, the determination of α_s using the heavier jet mass, $M_H^{(T)}$ is considered. This quantity is the mass of the heavier hemisphere in each event, where the event is divided according to the thrust axis (determined using all final state particles). The fits to the data obtained using the fixed order $\mathcal{O}(\alpha_s^2)$ calculation and also the combination of $\mathcal{O}(\alpha_s^2)$+resummed NLLA calculations are given in Fig. 9, along with the measured data. The resummed calculations give a much improved fit to the data over a wider range of $M_H^{(T)}$, especially in the softer regions of the distribution. The value of $\Lambda_{\overline{MS}}$ from this fit (with

$x_\mu = 1$) is closer to that from the fixed $\mathcal{O}(\alpha_s^2)$ calculation in which x_μ was allowed to vary, which supports the notion that scale optimisation reduced the effect of higher order contributions.

The results from the two fits are,

$$\mathcal{O}(\alpha_s^2) + \text{NLLA}, \qquad \alpha_s(M_{Z^0}) = 0.117 \pm 0.005$$
$$\mathcal{O}(\alpha_s^2) \text{ alone}, \qquad \alpha_s(M_{Z^0}) = 0.129 \pm 0.010$$

4.5. Determinations of α_s based on $\mathcal{O}(\alpha_s^3)$ QCD

In addition to the pure $\mathcal{O}(\alpha_s^2)$ calculations and the matched calculations $\mathcal{O}(\alpha_s^2)$+NLLA, predictions for two very inclusive observables are available to $\mathcal{O}(\alpha_s^3)$, both of which are used to determine α_s. The calculations describe the ratio of the hadronic and the leptonic decay widths of the Z^0 [28] and the ratio of the hadronic and electronic branching fractions of the τ lepton [29, 30]. Similar techniques are used in both calculations.

4.5.1. Example of $\mathcal{O}(\alpha_s^3)$ determination of α_s: R_τ

The prediction in $\mathcal{O}(\alpha_s^3)$ [29, 30] used describes the ratio of branching ratios of the τ lepton in the form,

$$R_\tau = \frac{B(\tau \to \text{hadrons} + \nu_\tau)}{\text{B}(\tau \to \text{e}\bar{\nu}_\text{e}\nu_\tau)}.$$

This may be expressed in an equivalent form, replacing the hadronic branching fraction by $1 - B(\tau \to \text{e}, \mu)$. The individual branching fractions to electrons and muons may in turn be replaced by approximately twice[6] the electronic branching ratio. By assuming lepton universality and combining the electronic and muonic branching fractions, a more precise experimental measurement is possible. The resulting form for R_τ is,

$$R_\tau = \frac{1 - 1.9728B(\tau \to \text{e}\bar{\nu}_\text{e}\nu_\tau)}{\text{B}(\tau \to \text{e}\bar{\nu}_\text{e}\nu_\tau)} = 3.795 \pm 0.119 \pm 0.111.$$

The theoretical expression for this quantity may be written,

$$R_\tau = 3(|V_{ud}|^2 + |V_{us}|^2)(1 + \delta_{\text{pert}} + \delta_{\text{non-pert}} + \delta_{\text{EW}}),$$
$$= 3.000(1.019 + \delta_{\text{pert}} + \delta_{\text{non-pert}}),$$

[6] The small deviation from 2 is due to the slightly reduced phase space available for the decay $\tau \to \mu$ compared with the decay $\tau \to$ e.

where $\delta_{\mathrm{non-pert}} = -0.010 \pm 0.004$ and δ_{pert} is calculated to $\mathcal{O}(\alpha_s^3)$. By comparing the $\mathcal{O}(\alpha_s^2)$ and $\mathcal{O}(\alpha_s^3)$ terms, varying the renormalisation scale in the range $1.0 \leq \mu \leq 2.5$ GeV (encompassing the c quark production threshold) and taking the number of active quark flavours, $n_f = 3$, the coupling parameter determined (at the τ mass scale) is

$$\alpha_s(M_\tau) = 0.389^{+0.077}_{-0.075}, \qquad (\text{in } \mathcal{O}(\alpha_s^3)),$$

where the overall error includes the contributions from experiment, non-perturbative effects and uncertainty in the renormalisation scale.

4.5.2. Consistency tests

This measurement can be compared with the other α_s measurements performed by extrapolating the value $\alpha_s(M_\tau)$ to $\alpha_s(M_{Z^0})$ using the appropriate form of the renormalisation group equation [41]. The coupling $\alpha_s(\mu)$ is assumed to be continuous which implies that $\Lambda_{\overline{MS}}$ is a step function at quark production thresholds. The lack of knowledge about the precise scale at which a quark flavour becomes active is dealt with by assuming that it happens at a scale in the range $M_q \leq \mu \leq 2M_q$, where M_q represents the mass of a given quark flavour. The extrapolation is carried out assuming flavours become active at $\mu = M_q$ and then repeated assuming the production threshold is at $\mu = 2M_q$. The average of these results gives the central value and half of their difference is taken to be the systematic error from the extrapolation.

The final result from the R_τ measurement (at the Z^0 mass scale) is found to be,

$$\alpha_s(M_{Z^0}) = 0.123^{+0.006}_{-0.007} \qquad (\text{in } \mathcal{O}(\alpha_s^3)).$$

4.6. Summary of α_s measurements and conclusions

This analysis presents the D scheme jet rates for the first time in an experimental investigation. It uses the recent resummed NLLA calculations for the observables T, $M_H^{(T)}$ and $M_H^{(M)}$. It includes the first experimental results of the PTEC and the jet mass observables $M_H^{(M)}$ and $M_D^{(M)}$ at Z^0 energies. The strong coupling parameter has been determined using 13 different observables at $\mathcal{O}(\alpha_s^2)$, using 3 different observables and resummed NLLA calculations, and using 2 observables at $\mathcal{O}(\alpha_s^3)$. The experimental uncertainties from detector effects typically lead to an uncertainty in α_s of 1–4%. Statistical uncertainties, which are responsible for less than a 1% error in the final value of α_s, are no longer a limiting experimental consideration.

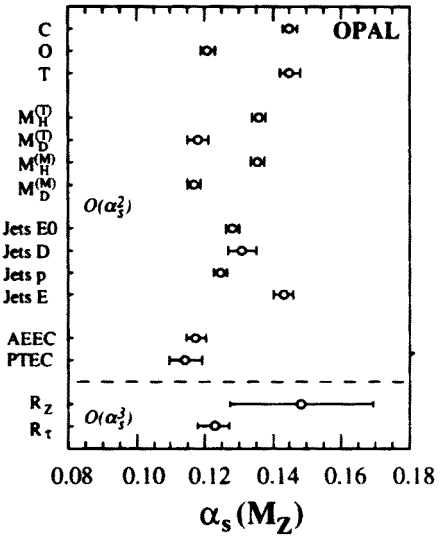

Fig. 10. Individual measurements for $\alpha_s(M_{Z^0})$, $\mu = M_{Z^0}$. The errors are from experimental systematic and statistical uncertainties only. No hadronisation or scale uncertainties are included.

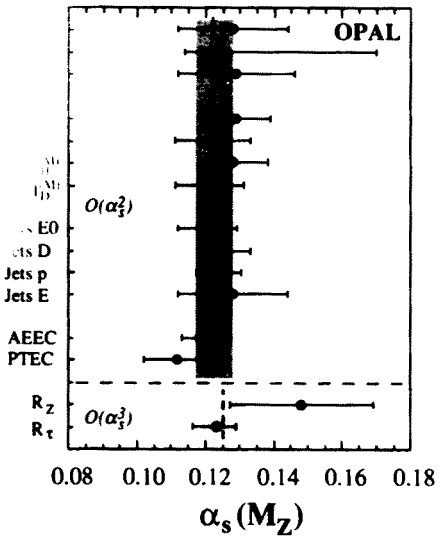

Fig. 11. Final measurements for $\alpha_s(M_{Z^0})$, for each observable. The errors include hadronisation and scale uncertainties. Shaded bands correspond to the weighted averages from the $\mathcal{O}(\alpha_s^2)$ measurements (upper) and from the $\mathcal{O}(\alpha_s^3)$ measurements (lower).

The measurements of α_s made using the fixed order calculations with

the different observables are shown in Fig. 10. These results are from fits to the data in which the renormalisation scale parameter had the value $x_\mu = 1$. The errors quoted are purely experimental and no account has been taken of the renormalisation scale or hadronisation uncertainties. One should note that different observables may have widely differing higher order effects. It is clear from the figure that the different measurements are not consistent with a single value of α_s when only experimental uncertainties are considered.

By contrast, Fig. 11 shows the measurements after the effects of hadronisation and renormalisation scale uncertainty have been included. The values determined are consistent with there being a single value for $\alpha_s(M_{Z^0})$ for all measurements, which is a necessary requirement of perturbative QCD, if the theory is to be correct. The consistency of the R_τ measurement with the other determinations is a new and largely independent check of QCD over a sizable interval in the renormalisation scale. Theoretical uncertainty now emerges as the dominant error in the experimental determination of the strong coupling parameter, α_s

Although the coupling determined using the resummed calculations is in good agreement with the fixed $\mathcal{O}(\alpha_s^2)$ and $\mathcal{O}(\alpha_s^3)$ calculations, it is not incorporated into the final result. This is because there are few such calculations available as yet and those which are available are for highly correlated observables. Furthermore, the procedure used to combine the NLLA calculations with the fixed $\mathcal{O}(\alpha_s^2)$ calculations needs to be more thoroughly studied and understood before it can be used with the same degree of confidence as the $\mathcal{O}(\alpha_s^2)$ calculations. For lack of similar calculations, the $\mathcal{O}(\alpha_s^3)$ determinations are not included in the final result. The results from these different types of calculation are treated as a good consistency check on the fixed $\mathcal{O}(\alpha_s^2)$ result. The final result for the strong coupling parameter from this study is therefore,

$$\alpha_s(M_{Z^0}) = 0.122^{+0.005}_{-0.006} \qquad (\text{in } \mathcal{O}(\alpha_s^2)).$$

5. Study of two-particle momentum correlations

This is a published analysis, based on approximately 500 000 hadronic events from the 1990 and 1991 data sample. Full details are available in the literature [4].

5.1. Introduction

Perturbative QCD calculations at high energies are normally carried out by either an order-by-order evaluation of Feynman diagrams or within the

framework of the leading logarithm approximation. At the present time, the full QCD matrix elements to $\mathcal{O}(\alpha_s^2)$ are known, allowing final states consisting of at most four partons to be modelled. This method is suitable for hard QCD processes, where the radiated gluons are few in number and energetic. In softer processes, where multiple gluon emission can not be neglected, this approach is less appropriate than the LLA method.

In an earlier investigation [42], it was shown that the measured momentum spectrum of soft particles could be related to LLA calculations which described the corresponding distribution for soft gluons, within a normalisation factor. To make this comparison, the hypothesis of "local parton hadron duality" LPHD [43] has to be invoked, which postulates that the distribution of hadrons should be approximately the same as that of partons, which is equivalent to the assertion that hadronisation has only a small effect upon the measured spectrum. The distribution measured in [42] is that of

$$D(\xi) = \frac{1}{\sigma}\frac{d\sigma}{d\xi},$$

where $\xi = \ln(1/x_p)$, $x_p = 2p/\sqrt{s}$, p is the particle momentum and σ is the observed cross section.

It was found in [42] that both the shape and the peak position of the data were well described by analytic QCD. It was noted that the analytic QCD prediction and the data exhibited an approximately gaussian form, with a peak position of $\xi \simeq 3,6$, corresponding to a particle momentum of typically 1.2 GeV. The treatment of coherence effects between soft gluons was found to be important for the calculations to describe the data well.

This study concentrates on comparing data with a recent extension of the earlier calculations [44] to a two-particle momentum distribution. This description of this study begins by introducing the correlation function for which the theoretical predictions have been made, followed by a brief outline of the experimental procedure. Comparisons with analytic QCD predictions and also with coherent and incoherent parton shower models are made. Finally, the results of the comparisons are summarised and some conclusions are presented.

5.2. Correlation function

The two-particle momentum correlation function to be studied is defined,

$$R(\xi_1, \xi_2) = \frac{D^{(2)}(\xi_1, \xi_2)}{D^{(1)}(\xi_1)D^{(1)}(\xi_2)},$$

with,

$$D^{(1)}(\xi) = \frac{1}{\sigma}\frac{d\sigma}{d\xi}, \qquad D^{(2)}(\xi_1, \xi_2) = \frac{1}{\sigma}\frac{d^2\sigma}{d\xi_1 d\xi_2}.$$

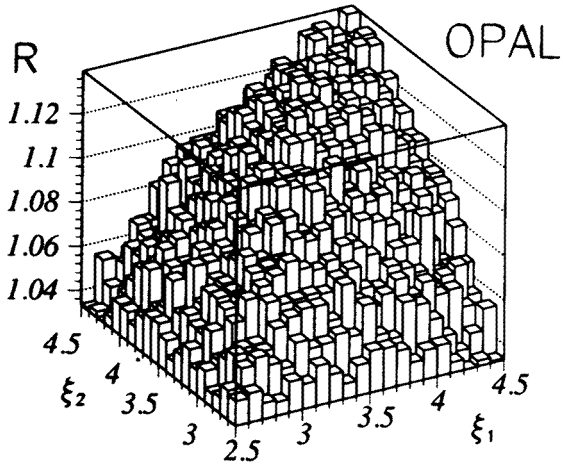

Fig. 12. The experimentally measured two-particle momentum correlation function, $R(\xi_1, \xi_2)$, corrected for detector effects.

This function is evaluated using the measured data and is shown in Fig. 12. The region of $\xi_{1,2}$ for which this R is shown corresponds to particle momenta in the range 3.8–0.5 GeV. A positive correlation is seen in the figure, increasing towards lower momenta (higher $\xi_{1,2}$).

The analytic NLLA calculation of [44] predicts a correlation function of the form,

$$R(\xi_1, \xi_2) = c_1 + c_2(\xi_1 + \xi_2) + c_3(\xi_1 - \xi_2)^2 , \tag{3}$$

with,

$$c_1 = 1.375 - \frac{1.262}{(\ln(Q/\Lambda))^{\frac{1}{2}}} ; \quad c_2 = \frac{0.877}{(\ln(Q/\Lambda))^{\frac{3}{2}}} ; \quad c_3 = -\frac{1.125}{(\ln(Q/\Lambda))^2} .$$

A much earlier calculation of this function in leading order [45] predicted that the terms c_i of Eq. (3) would have the values 1.375 and 0 for c_1 and c_2, respectively, whilst c_3 would be the same as was calculated in next-to-leading order. A linear increase in R for increasing $\xi_1 + \xi_2$ is a feature predicted by the next-to-leading calculation that is absent from the leading order calculation. One should note that the scale, Λ in the recent calculation is some effective QCD scale — the current calculation are of too low an order for this to corresponds to $\Lambda_{\overline{MS}}$.

5.3. Experimental considerations

The choice of momentum interval for the analysis is restricted by the both theory and experiment. For particle momenta much higher than 4 GeV

the LLA approach is not ideal as this is tending towards the region of hard processes, where matrix element calculations are more appropriate. For particle momenta much less than 0.5 GeV, kinematics and mass effects have to be considered. These considerations define a natural region inside which the analysis is carried out.

An attractive feature of the two-particle correlation distribution is that many experimental uncertainties and systematic effects cancel out with one another. The measured distribution is still corrected for detector effects on a bin-by-bin basis, as in the α_s analyses. The correction factors evaluated are $\lesssim 1\%$. A systematic uncertainty in the correlation, $\Delta R \sim \pm 0.005$ is determined from the choice of the Monte Carlo model used to evaluate the corrections. The measured R is found to be insensitive to moderate variations in event and charged track selection criteria.

The data sample used includes all data available; being a two-dimensional function, the large dataset is essential. Significant additional material added in front of the tracking chambers after the 1990 run is adequately modelled in the detector simulation, giving consistently good agreement with data. The 1990 and 1991 samples are combined after weighting and analysed together.

The comparison of data with both calculation and models is carried out by concentrating upon narrow bands of R in the (ξ_1, ξ_2) plane. The analytic form for R is compared with and fitted to the measured, corrected data. The expectation from various Monte Carlo models is also compared with the data. The specific regions presented herein are,

(a) $|\xi_1 - \xi_2| < 0.1$,

(b) $6.9 < \xi_1 + \xi_2 < 7.1$,

which are across the two diagonals in the (ξ_1, ξ_2) shown in Fig. 12.

5.4. Comparison with analytic QCD calculations

The corrected data and the analytic prediction for various values of the QCD scale, Λ, are illustrated in Fig. 13. The next-to-leading order calculations reproduce the same general trends as are present in the data, *i.e.* R increases with $\xi_1 + \xi_2$ and is largest for $\xi_1 \approx \xi_2$. The data tend to support the next-to-leading prediction for a linear increase in R with $\xi_1 + \xi_2$, which the leading order prediction does not cater for. In trying to fit R to the data with each of the parameters, c_i freely varying, poor χ^2/d.o.f. were found and the values of λ obtained were not consistent with one another. This suggests that either the next, higher order terms are important (they might be expected to have an effect of similar magnitude to the difference between leading and next-to-leading predictions), or that the calculation is incorrect.

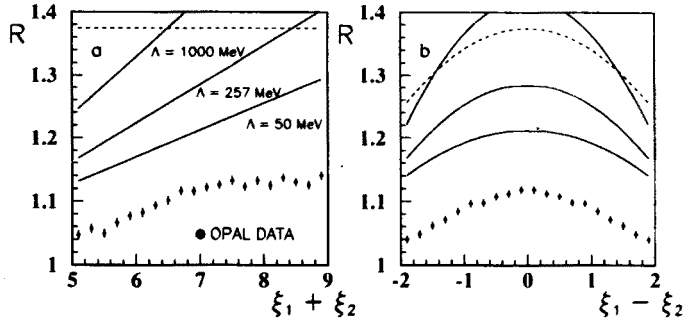

Fig. 13. Comparison of corrected data with NLLA analytic calculations, for various QCD scales, Λ. Solid curves are next-to-leading predictions, dashed curve is leading order prediction, for $\Lambda = 255$ MeV.

5.5. *Comparison with coherent parton shower models*

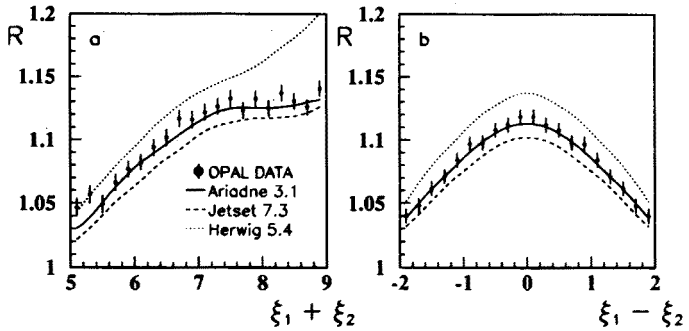

Fig. 14. Comparison of corrected data with coherent, parton shower models.

Three coherent parton shower models are compared with the data, *viz.*

- JETSET [19], with string fragmentation,
- HERWIG [35] with cluster fragmentation, and
- ARIADNE [46] with a colour dipole formulation of the parton shower and string fragmentation.

These models have been tuned to OPAL global event shape distributions and consequently, there are uncertainties on the model parameters. Within the uncertainties arising from the tuning procedure, there is no substantial disagreement with the observed data.

5.6. *Comparison with incoherent parton shower models*

Having seen that the coherent parton shower models provide a reasonable description of the experimental data, two incoherent models are compared next, *viz.*

- JETSET, no coherence, with string fragmentation,
- COJETS, two versions, with incoherent parton shower and independent fragmentation.

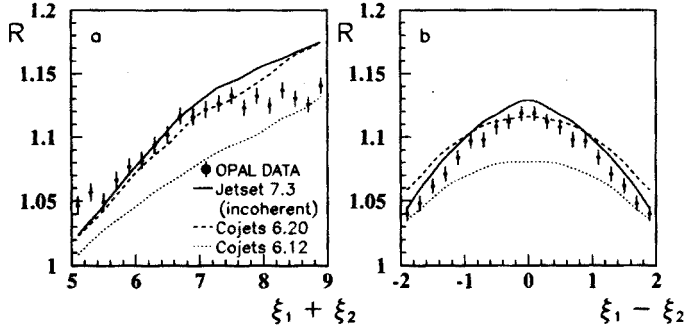

Fig. 15. Comparison of corrected data with incoherent, parton shower models.

These incoherent models do not describe the data particularly well. However, JETSET and COJETS 6.20 may be regarded as describing the data at least as well as the coherent HERWIG model. The possibility that the correlation observed may be due to non-perturbative effects such as Bose-Einstein correlation or resonance decays has been investigated using the JETSET model. These studies indicate that these effects are not significant. The fact that the JETSET $\mathcal{O}(\alpha_s^2)$ matrix element Monte Carlo, which would only include a small fraction of any soft coherence effects, can describe the data moderately well (when string fragmentation is used), implies that much of the effect observed comes from the string hadronisation in these models.

5.7. Summary and conclusions

This study presents for the first time two-particle momentum correlations at small x_p in e^+e^- annihilation. A positive correlation has been observed in the data. There is some tendency for the data to support the next-to-leading analytic calculation, but the calculations at the present time do not truly describe the data. The arbitrary normalisation which is an artifact of the LPHD hypothesis in the one-dimensional momentum distribution cancels in the two-particle case. This distribution may therefore be regarded as a more stringent test of QCD than the corresponding single-particle distribution.

The observed correlation is seen to lie significantly below the analytic calculation for any reasonable value of Λ. Some similarity appears to exist between the momentum spectra and the multiplicity distributions. In the

latter, the average multiplicity distribution (cf. one-particle momentum distribution) is well described by the next-to-leading calculation. In the case of the second binomial moment of the multiplicity (cf. two-particle momentum distribution), the next-to-leading calculation cannot be reasonably made to fit the data.

It is concluded that higher order effects are absorbed into the hadronisation process in the Monte Carlo models, allowing them to describe the data (at the hadron level), even though they disagree with each other at the parton level. Assuming that LPHD is a reasonable hypothesis to apply to this distribution, and that the calculations are correct, it seems that yet higher order terms will be required in order to improve the description of the data.

6. Overall summary

This report has described a study in which the electric charge of quarks and gluons are found to cause significant differences in the measured jet charge distributions.

It has described a detailed analysis of $\alpha_s(M_{Z^0})$ in which many observables have been used. All of the measured data can be consistently described by a single value of the strong coupling parameter, α_s, as predicted by QCD. The dominant source of uncertainty is now theoretical and more resummed and higher order calculations are required in order to improve upon the current measurements.

Finally, a positive correlation has been observed in two-particle momentum distributions. There is some indication that the data supports the predictions of the next-to-leading order LLA calculations,

I would like to thank the conference organisers for their hard work and hospitality in running an enjoyable and stimulating conference, and providing a friendly atmosphere in which to discuss physics.

REFERENCES

[1] P. Ward, *Precision Tests of the Standard Model at LEP*, Invited talk given at the XVth International Warsaw Meeting on Elementary Particle Physics, Kazimierz, 25-29th May 1992.
[2] OPAL Collab., OPAL Physics Note PN058, 17th March, 1992, unpublished.
[3] OPAL Collab., P.D. Acton *et al.*, *Z. Phys.* **C55**, 1 (1992).
[4] OPAL Collab., P.D. Acton *et al.*, *Phys. Lett.* **B287**, 401 (1992).
[5] OPAL Collab., K. Ahmet *et al.*, *Nucl. Instr. and Meth.* **A305**, 275 (1991).
[6] OPAL Collab., P.D. Acton *et al.*, *Phys. Lett.* **B276**, 379 (1992).

[7] OPAL Collab., P.D. Acton *et al.*, *Phys. Lett.* **B276**, 547 (1992).
[8] OPAL Collab., P.D. Acton *et al.*, *Phys. Lett.* **B278**, 485 (1992).
[9] ALEPH, DELPHI, L3 and OPAL, *Phys. Lett.* **B276**, 247 (1992).
[10] OPAL Collab., P.D. Acton *et al.*, *Phys. Lett.* **B281**, 405 (1992).
[11] OPAL Collab., P.D. Acton *et al.*, *Phys. Lett.* **B281**, 394 (1992).
[12] OPAL Collab., P.D. Acton *et al.*, *Z. Phys.* **C55**, 191 (1992).
[13] OPAL Collab., P.D. Acton *et al.*, *Phys. Lett.* **B287**, 389 (1992).
[14] OPAL Collab., P.D. Acton *et al.*, CERN-PPE/92-66, submitted to *Phys. Lett.* **B**.
[15] R.D. Field, R.P. Feynman, *Nucl. Phys.* **B136**, 1 (1978).
[16] OPAL Collab., M.Z. Akrawy *et al.*, *Phys. Lett.* **B261**, 334 (1991).
[17] OPAL Collab., G. Alexander *et al.*, *Phys. Lett.* **B265**, 462 (1991).
[18] OPAL Collab., M.Z. Akrawy *et al.*, *Z. Phys.* **C49**, 375 (1991).
[19] T. Sjöstrand, *Comp. Phys. Comm.* **39**, 347 (1986); T. Sjöstrand, *Comp. Phys. Comm.* **43**, 367 (1987); M. Bengtsson, T. Sjöstrand, *Nucl. Phys.* **B289**, 810 (1987); B. Andersson, G. Gustafson, G. Ingelman, T. Sjöstrand, *Phys. Rep.* **97**, 31 (1983).
[20] OPAL Collab., M.Z. Akrawy *et al.*, *Z. Phys.* **C47**, 505 (1990).
[21] OPAL Collab., J. Allison *et al.*, *Nucl. Inst. and Meth.* **A317**, 47 (1992).
[22] UA1 Collab., G. Arnison *et al.*, *Nucl. Phys.* **B276**, 253 (1986).
[23] JADE Collab., T. Greenshaw *et al.*, *Z. Phys.* **C42**, 1 (1989).
[24] Z. Kunszt, P. Nason [conv.], in *Z. Physics at LEP 1*, eds. G. Altarelli, R. Kleiss and C. Verzegnassi, CERN 89-08, 1989.
[25] R.K. Ellis, D.A. Ross, A.E. Terrano, *Nucl. Phys.* **B178**, 421 (1981).
[26] S. Catani, L. Trentadue, G. Turnock, B.R. Webber, *Phys. Lett.* **B263**, 491 (1991).
[27] S. Catani, G. Turnock, B.R. Webber, *Phys. Lett.* **B272**, 368 (1991).
[28] S.G. Gorishny, A.L. Kataev, S.A. Larin, *Phys. Lett.* **B259**, 144 (1991); L.R. Surguladze, M.A. Samuel, *Phys. Rev. Lett.* **66**, 560 (1991); Erratum, *Phys. Rev. Lett.* **66**, 2416 (1991).
[29] E. Braaten, *Phys. Rev. Lett.* **60**, 1606 (1988).
[30] E. Braaten, S. Narison, A. Pich, *Nucl. Phys.* **B373**, 581 (1992).
[31] P.M. Stevenson, *Phys. Rev.* **D24**, 1622 (1981).
[32] S.J. Brodsky, G.P. Lepage, P.B. Mackenzie, *Phys. Rev.* **D28**, 228 (1983).
[33] G. Grunberg, *Phys. Lett.* **B95**, 70 (1980); Erratum *Phys. Lett.* **B110**, 501 (1982).
[34] J. Ellis, D.V. Nanopoulos, D.A. Ross, *Phys. Lett.* **B267**, 132 (1991).
[35] G. Marchesini, B.R. Webber, *Nucl. Phys.* **B310**, 461 (1988); G. Marchesini, B.R. Webber, Cavendish-HEP-88/7.
[36] R. Odorico, *Comp. Phys. Comm.* **32**, 139 (1984); R. Odorico, *Comp. Phys. Comm.* **59**, 527 (1990).
[37] Particle Data Group, *Review of Particle Properties*, *Phys. Rev.* **D45**, I.1 (1990).
[38] JADE Collab., W. Bartel *et al.*, *Z. Phys.* **C33**, 23 (1986); JADE Collab., S. Bethke *et al.*, *Phys. Lett.* **B213**, 235 (1988).

[39] N. Brown, W.J. Stirling, *Phys. Lett.* **B252**, 657 (1990).
[40] S. Bethke, Z. Kunszt, D. Soper, W.J. Stirling, *Nucl. Phys.* **B370**, 310 (1992); S. Catani *et al.*, *Phys. Lett.* **B269**, 432 (1991); N. Brown, W.J. Stirling, *Z. Phys.* **C53**, 629 (1992).
[41] W.J. Marciano, *Phys. Rev.* **D29**, 580 (1984).
[42] OPAL Collab., M.Z. Akrawy *et al.*, *Phys. Lett.* **B247**, 617 (1990).
[43] D. Amati, G. Veneziano, *Phys. Lett.* **B83**, 87 (1979); Ya.I. Azimov, Yu.L. Dokshitzer, V.A. Khoze, S.I. Troyan, *Z. Phys.* **C27**, 65 (1985).
[44] C.P. Fong, B.R. Webber, *Nucl. Phys.* **B355**, 54 (1991); C.P. Fong, *Ph.D. Thesis*, University of Cambridge, October 1991.
[45] Yu.L. Dokshitzer, V.S. Fadin, V.A. Khoze, *Z. Phys.* **C18**, 37 (1983).
[46] U. Pettersson, LU TP 88-5 (1988); L. Lönnblad, U. Pettersson, LU TP 88-15 (1988); L. Lönnblad, LU TP 89-10 (1988).